Peer-reviewed version available at Int. J. Mol. Sci. 2020, 21, 5654; doi:10.3390/ijms21165654

Tuning of Molecular Electrostatic Potential Enables Efficient Charge Transport in Crystalline Azaacenes: A Computational Study

Andrey Yu. Sosorev[1,2]*, Dmitry I. Dominskiy[3], Ivan Yu. Chernyshov[4], Roman G. Efremov[1]

1. *Shemyakin-Ovchinnikov Institute of bioorganic chemistry of the Russian Academy of Sciences, Ulitsa Miklukho-Maklaya, 16/10, Moscow, GSP-7, 117997, Russia*
2. *Institute of Spectroscopy of the Russian Academy of Sciences, Fizicheskaya Str., 5, Troitsk, Moscow 108840, Russia*
3. *Faculty of Physics and International Laser Center, Lomonosov Moscow State University, Leninskie Gory 1/62, Moscow 119991, Russia*
4. *TheoMAT Group, ChemBio cluster, ITMO University, Lomonosova 9, St. Petersburg 191002, Russia*

**e-mail: sosorev@physics.msu.ru*

Abstract

Chemical versatility of organic semiconductors provides nearly unlimited opportunities for tuning their electronic properties. However, despite decades of research, relationship between molecular structure, molecular packing and charge mobility in these materials remains poorly understood. This reduces the search for high-mobility organic semiconductors to the inefficient trial-and-error approach. For clarifying the abovementioned relationship, investigations of the effect of small changes in the chemical structure on OSs properties are particularly important. In this study, we address computationally the impact of substitution of C-H atom pairs by nitrogen atoms (N-substitution) on molecular properties, molecular packing and charge mobility of crystalline oligoacenes. Besides of decreasing frontier molecular orbital levels, N-substitution dramatically alters molecular electrostatic potential yielding pronounced electron-rich and electron-deficient areas. These changes in the molecular electrostatic potential strengthen face-to-face and edge-to-edge interactions in the corresponding crystals and result in the crossover from the herringbone packing motif to π-stacking. When the electron-rich and electron-deficient areas are large, sharply defined and, probably, have certain symmetry, charge mobility increases up to 3-4 $cm^2V^{-1}s^{-1}$. The results obtained highlight the potential of azaacenes for application in organic electronic devices and are expected to facilitate rational design of organic semiconductors for steady improvement of organic electronics.

Keywords:

Organic electronics, organic semiconductors, molecular design, crystal design, π-stacking, charge mobility

Introduction

Organic semiconductors with efficient charge transport, i.e. high charge mobility μ, are of great demand for organic electronics. However, only several organic semiconductors (OSs) with μ>1 $cm^2V^{-1}s^{-1}$ have been discovered [1, 2]. Nevertheless, the tunability of the molecular structure of OSs [1] gives a hope for finding novel high-mobility materials among them. Unfortunately, search for high-mobility OSs still relies mainly on the trial-and-error approach, and design rules that could direct and rationalize this search are highly desirable.

OSs consist of π-conjugated molecules held together by the intermolecular forces [3, 4]. The molecular nature of the OSs limits the charge transport in these materials: although charge carriers (electrons or holes) are efficiently delocalized within the molecules, their intermolecular

delocalization or transfer from one molecule to another is generally hindered by the weakness of the electronic interaction between the molecules [3, 4]. Specifically, local and non-local electron-vibrational (electron-phonon) interaction quantified by reorganization energy λ and lattice distortion energy, respectively, overwhelm intermolecular electronic interaction quantified by the charge transfer integrals J, and induce charge localization. As a result, charge transport proceeds via inefficient hopping mechanism; the hopping rate increases with J and decreases with λ [5, 6, 7]. Nevertheless, if J are sufficiently large, significant intermolecular charge delocalization resulting in efficient bandlike charge transport can take place [5, 8, 9]. Thus, increasing J and decreasing λ is important for improvement of charge mobility in OSs.

The λ values can be readily predicted from just the molecular structure [9]. On the contrary, prediction of J values from just the molecular structure seems to be not feasible yet. Indeed, the J values are determined by the relative positions of the molecules and are very sensitive to the latter [10]. Thus, prediction of J requires reliable modeling of molecular arrangement; for crystalline OSs, to which record-μ OSs belong and which we will focus on, this means prediction of the crystal structure. Unfortunately, reliable crystal structure prediction for OSs is not straightforward and yet remains hardly feasible [11, 12, 13], precluding the desired assessment of J and hence μ just from the molecular structure. In this context, semiempirical "rules-of-thumb" linking the molecular structure, crystal structure and charge transport properties are of significant importance.

The formation of molecular crystals is guided by the avoidance of a vacuum, the lessening of repulsive intermolecular interactions, as well as the boosting of attractive molecular forces [11]. There are two major types of molecular packing motifs in crystalline OSs: herringbone and π-stacking (the latter is sometimes divided into slipped stack and brick-wall arrangements [1]). In herringbone-type crystals, the molecular planes of the adjacent molecules are tilted with respect to each other due to the preference of edge-to-face CH···π interactions over face-to-face π···π and edge-to-edge H···H ones. This is maintained by the electrostatic interaction between slightly electron-deficient (bearing partial positive charge) hydrogen atoms and electron-rich (bearing partial negative charge) π-conjugated core [6, 14]. In π-stacking packing motif, the molecules are arranged parallelly – in the face-to-face manner, – and π-conjugated systems of the molecules can significantly overlap. This packing is realized if face-to-face and edge-to-edge interactions overwhelm edge-to-face interactions [15] due to either altered electrostatics or steric hindrance induced by bulky side groups [16, 17, 18]. It was noticed that the largest J are generally observed for face-to-face arrangement typical for π-stacking packing motif [13, 19]. For instance, in the OSs with record μ, e.g., crystalline rubrene (hole transport)[20] and F_2-TCNQ (electron transport) [21], the largest J are observed for face-to-face orientation of adjacent molecules and amount ~70-110 meV, which is significantly larger than the energy of thermal fluctuations (25 meV at room temperature) [8]. For this reason, crystalline OSs with π-stacking attracted particular attention in the last decades.

One of the strategies for designing crystals with π-stacking is the introduction of electron-withdrawing groups (EWG), especially cyano-groups and halogen (e.g. fluorine) atoms. There are two reasons for the structural changes induced by these groups. The first reason is the strengthening of edge-to-edge interactions due to CH···EWG contacts, e.g., CH···F and CH···NC [15]. The second reason is the enhancement of face-to-face π···π interactions due to the formation of electron-deficient and electron-rich parts of a π-system as a result of electron density redistribution [17, 19]. Note that introduction of EWG can sometimes result in the opposite structural changes: extensive fluorination can induce the crossover to the herringbone structure from the π-stacking one [19, 21, 22]. Insertion of heteroatom directly in the conjugated core, e.g. substitution of CH with N (N-substitution), can be another way of tuning the crystal structure: this substitution also weakens edge-to-face interactions and facilitates edge-to-edge and face-to-face interactions [13, 23-25]. However, this molecular structure modification is much less common in the design of OSs as compared to fluorination and cyano-substitution, and its effect is worth detailed investigation. Nevertheless, N-substitution could be more beneficial for charge transport than halogenation since in the former case, "electronically insulating" hydrogen and halogen atoms

are removed from the molecular structure, and N atoms bearing the π-electron density come in "conductive" contact with the π-conjugated systems of the nearby molecules [15].

A convenient playground for studying the impact of N-substitution on the crystal structure and properties is the series of oligoacenes – one of the most studied classes of OSs. Accordingly, comparison of the oligoacenes and their N-substituted counterparts – azaacenes – was performed in several studies [13, 23, 25]. It was observed that while oligoacenes favor herringbone crystal packing [27], their N-substituted counterparts can show π-stacking packing motif [23-26]. In line with reasoning provided above, changes in the crystal structure were attributed to the changes in the electrostatic potentials of the oligoacene molecules with N-substitution and emergence of CH···N weak hydrogen bonds [23, 24]. Nevertheless, a systematic study of the effect of N-substitution on the crystal packing of various oligoacenes is lacking. For instance, molecular packing and charge transport in crystalline azaacenes with more than two nitrogen atoms were not addressed theoretically before.

Similarly, the effect of N-substitution on the charge-transport properties is also poorly studied. Oligoacenes show considerable hole mobilities [2, 28]; however, electron transport in them is not observed in organic field-effect transistors (OFETs) because of the high lowest unoccupied molecular orbital (LUMO) levels preventing electron injection [2]. N-substitution decreases LUMO levels and can result in efficient electron transport [26, 29]. However, according to the findings of Winkler and Houk [30], as many as seven nitrogen atoms are to be introduced in the pentacene core to enable electron conductivity with commonly used electrodes. To the best of our knowledge, pentacene derivatives with maximum four nitrogens were synthetized to date; luckily, they already show electron conduction [26]. We have no data concerning the tests of the lower azaacenes, e.g. azaanthracenes or azatetracenes, in field-effect devices. Thus, theoretical assessment of the highest occupied molecular orbital (HOMO) and LUMO levels, as well as electron and hole mobility in various azaacenes, is of significant interest.

In this study, we address computationally the impact of N-substitution on the properties of individual molecules, crystal structure and charge mobility of the most popular oligoacenes – anthracene, tetracene and pentacene. The role of the number and position of the nitrogen heteroatoms in the mentioned π-conjugated cores is systematically analyzed. Only azaacenes without side groups that were successfully synthesized, and for which crystal structure is known, are considered; this distinguishes our study from the recent reports where predicted crystal structures were used [23, 24] or substituted azaacenes were addressed [31]. Furthermore, the molecular packing and charge transport in the crystals of azaacenes with four nitrogen atoms, which were not addressed theoretically before, are considered. We show that N-substitution facilitates π-stacking; in several cases (but not all), these changes in the molecular packing significantly improve charge transport. The positive effect of N-substitution on the charge mobility is most pronounced when the nitrogen atoms are arranged in the centrally symmetric pattern without plane of symmetry, and form large electronegative areas. This results in large hole transfer integrals (up to 85 meV) and very large electron transfer integrals (up to 175 meV), providing theoretical hole and/or electron mobilities exceeding 1 $cm^2V^{-1}s^{-1}$ for three OSs: 1,5,9,10-tetraazaanthracene (**4NA**), 6,13-diazapentacene (**2NP**) and 1,7,8,14-tetraazapentacene (**4NP**). Finally, we extend the obtained results on the nucleobases – natural π-conjugated compounds bearing multiple nitrogen atoms in the conjugated core. Our findings show that tailoring the pattern of N-substitution within the conjugated core can be used as a promising strategy for design of efficient organic semiconductors.

Materials and methods

Density functional theory (DFT) calculations for isolated molecules were performed using B3LYP density functional and 6-31g(d,p) basis set in the GAMESS package [32, 33]. Geometry optimization was performed prior to all calculations. Reorganization energies and charge transfer integrals were calculated at B3LYP/6-31g(d,p) and B3LYP/6-31g(d) levels, respectively. The reorganization energy for charge transport, λ, was approximated by its inner-sphere part, which is

typically considered much larger than the outer-sphere part [7]. The λ values for all the studied compounds were calculated according to the common potential energy surface (adiabatic potentials) scheme [7, 10, 34] from the energies of the molecule in the following four states: the neutral state in its optimized geometry (E_N), the neutral state in the optimized geometry of the charged state (E_N^*), the charged state in its optimized geometry (E_C), and the charged state in the geometry of the neutral state (E_C^*): $\lambda = (E_N^* - E_N) + (E_C^* - E_C)$. For two compounds, pentacene and diazapentacene, λ were also calculated using normal mode decomposition method [7, 34]. Charge transfer integrals J were calculated using a home-written code based on the dimer projection method (DIPRO) [35-37]. Raman spectra were calculated from static polarizabilities in the off-resonance regime.

Hirshfeld surface analysis and energy framework calculations were performed in CrystalExplorer17.5 software [38] at B3LYP/6-31g(d,p) level. For energy framework calculations, molecular shell with 3.8Å radius was generated around a central molecule, and the interaction energies (electrostatic, dispersion, and total) between the molecular pairs were calculated. The scale factors for benchmarked energies used for the construction of energy models were taken from Ref. [39]. Crystal structures were obtained from CCDC database; no further geometry optimization was performed. CCDC entry codes are listed in Supporting Information (SI), Table S1.

Preprints (www.preprints.org) | NOT PEER-REVIEWED | Posted: 8 July 2020 doi:10.20944/preprints202007.0149.v1

Peer-reviewed version available at Int. J. Mol. Sci. 2020, 21, 5654; doi:10.3390/ijms21165654

Results

Molecules

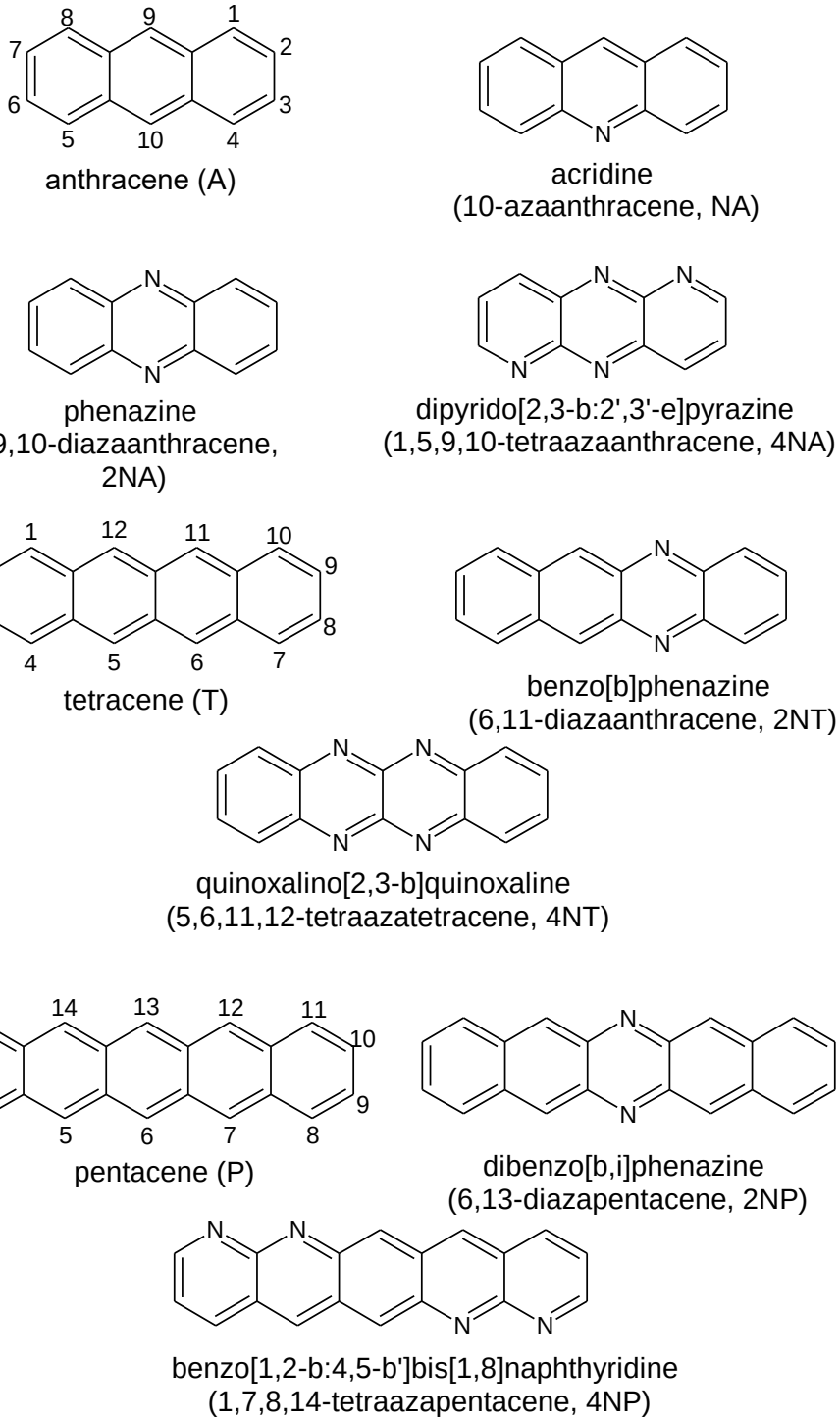

Figure 1. Chemical structure of the compounds studied.

Figure 1 presents the chemical structures of the compounds studied. These molecules fall into the three series: derivatives of anthracene (**A**), tetracene (**T**) and pentacene (**P**). In each of the series, the number of nitrogen atoms varies from 0 to 4. Figure 2 shows LUMO patterns and electrostatic potential (ESP) maps for **A** and its nitrogen-substituted derivatives: phenazine (9,10-diazaanthracene, or **2NA**) and dipyrido[2,3-b:2',3'-e]pyrazine (1,5,9,10-tetraazaanthracene, or **4NA**). LUMO patterns and ESP maps for the other compounds studied, as well as HOMO patterns for all the compounds studied are shown in Supporting Information (SI), Figures S1 and S2. From Figures 2, S1 and S2 it follows that N-substitution has negligible impact on LUMO pattern and

Preprints (www.preprints.org) | NOT PEER-REVIEWED | Posted: 8 July 2020 doi:10.20944/preprints202007.0149.v1

Peer-reviewed version available at *Int. J. Mol. Sci.* **2020**, *21*, 5654; doi:10.3390/ijms21165654

weakly affects HOMO pattern for all the compounds studied except for **4NA**. In the latter, HOMO pattern is qualitatively different from all the other compounds studied. In contrast to HOMO/LUMO patterns, ESP pattern is dramatically affected by N-substitution, in line with previous results [12, 24]. Specifically, while **A**, **T** and **P** have the electronegative center (carbon atoms) and the electropositive periphery (hydrogen atoms), the nitrogen atoms pull out the electron density resulting in emergence of strongly electronegative areas within the conjugated core and making the remaining part of the molecule (both carbon and hydrogen atoms) electropositive. Noteworthily, if nitrogen atoms are nearby (Figure 2e,h), the electronegative areas are large, and ESP pattern can consist of the "stripes" of alternating positive and negative ESP. One can expect that in crystal, the molecules will pack so that areas of positive ESP for one molecule will contact the areas of negative ESP for the other molecule according to the principle of ESP complementarity [14, 19]. Thus, the formed electron-rich and electron-deficient areas can direct the molecular arrangement in the crystals as will be described below.

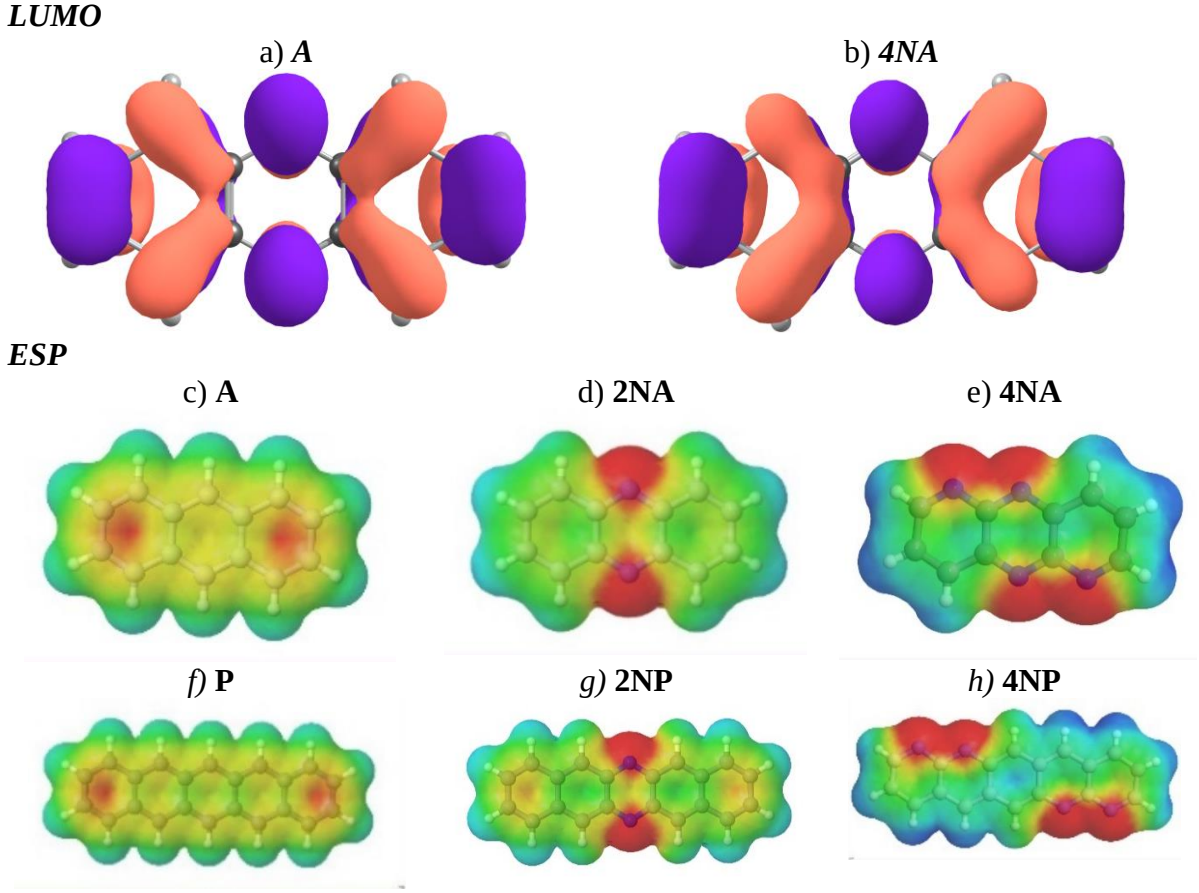

Figure 2. LUMO patterns (a,b) and ESP maps (c-g) for **A** (a,c), **2NA** (d), **4NA** (b,e), **P** (f) and **4NP** (g). Blue color in panels (c-h) designates strongly positive ESP, and red color designates strongly negative ESP. Green and yellow colors correspond to slightly positive and slightly negative ESP, respectively.

As expected, N-substitution lowers both the HOMO and LUMO energies. The HOMO-LUMO gap is weakly affected with substitution; for pentacene derivatives, it is the narrowest, while for anthracene derivatives, it is the widest. For **2NP**, **4NP**, **4NT** and **4NA**, LUMO energies are low enough to enable electron injection [26, 40], in line with observation of electron conductivity in diazapentacene in Ref. [26]. In contrast, **A**, **T**, **P**, **2NT** and **2NP** are expected to maintain efficient hole injection, in line with the results of Ref. [23]. Noteworthily, **2NP** can probably show ambipolar charge transport.

Preprints (www.preprints.org) | NOT PEER-REVIEWED | Posted: 8 July 2020 doi:10.20944/preprints202007.0149.v1

Peer-reviewed version available at Int. J. Mol. Sci. 2020, 21, 5654; doi:10.3390/ijms21165654

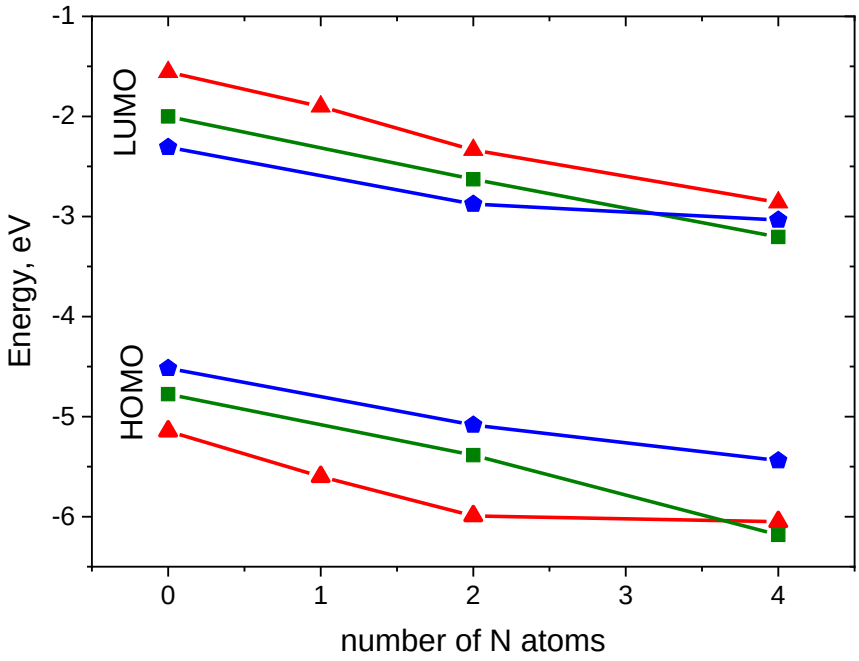

Figure 3. HOMO and LUMO energies for the compounds studied. Red triangles: **A** derivatives, green squares: **T** derivatives, blue pentagons: **P** derivatives.

Crystals

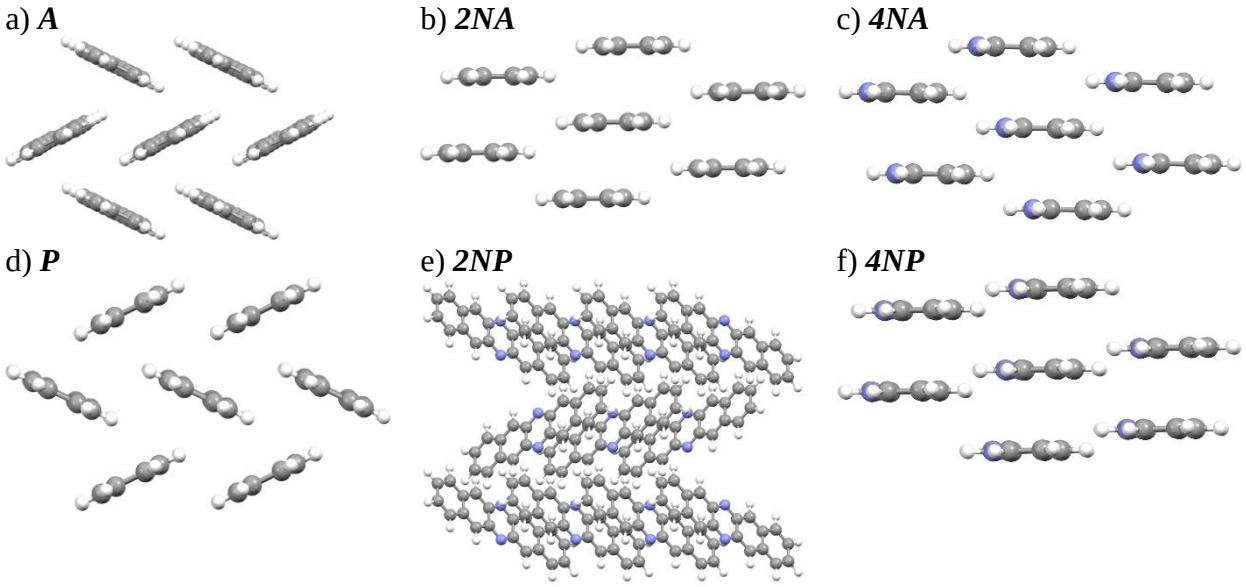

Figure 4. Crystal structures of the selected compounds.

Figure 4 presents the crystal structures of **A**, **P** and their selected N-substituted derivatives. From this figure it follows that while **A** and **P** show herringbone packing motif, **2NA, 2NP, 4NA** and **4NP** exhibit π-stacking. To illustrate and analyze the impact of nitrogen atoms on the molecular arrangement, we utilized Hirshfeld surface analysis of the crystal packing [41]. The Hirshfeld surface defines the space occupied by a molecule: inside this surface, the electron density from the given molecule is larger than that from the others [42]. Figures 5 and 6 show the Hirshfeld surfaces for the selected crystals from **A** and **P** series, respectively (for phenazine, only one polymorph was chosen), mapped with curvedness and ESP. Curvedness maps can be used to identify planar π-stacking arrangements [41]: the latter reveal themselves by relatively large green flat regions. The map for **A** (Figure 5a) has no such regions, which is typical for herringbone packing [41]. On the

Preprints (www.preprints.org) | NOT PEER-REVIEWED | Posted: 8 July 2020 doi:10.20944/preprints202007.0149.v1

Peer-reviewed version available at Int. J. Mol. Sci. 2020, 21, 5654; doi:10.3390/ijms21165654

contrary, the maps for **2NA** (Figure 5b) and **4NA** (Figure 5c) show one extended green region per face. This indicates π-stacking of the molecule with one adjacent molecule per its face (i.e., one-dimensional π-stacking) in these crystals. Similar situation is observed for pentacene and its N-substituted derivatives: while the curvedness map for **P** (Figure 6a) has no extended flat regions, for **2NP** and **4NP** (Figure 6b,c) such regions are observed, highlighting the crossover from the herringbone packing in the former crystal to the one-dimensional π-stacking in the two latter crystal. These changes are also revealed in the energy frameworks (see Figures S5, S8, S11): with N-substitution, certain (π-stacking) directions with large interaction energy emerge. Molecular ESPs in the crystals (Figure 5d-f; Figure 6d-f) directly inherit those of the single molecules (see Figure 1c-h): introducing nitrogen atoms into the conjugated core results in formation of extended electropositive and electronegative areas at the Hirshfeld surfaces. The latter areas facilitate electrostatic interactions between the molecules, which is also revealed in the energy frameworks diagrams (see Figures S5, S8, S11).

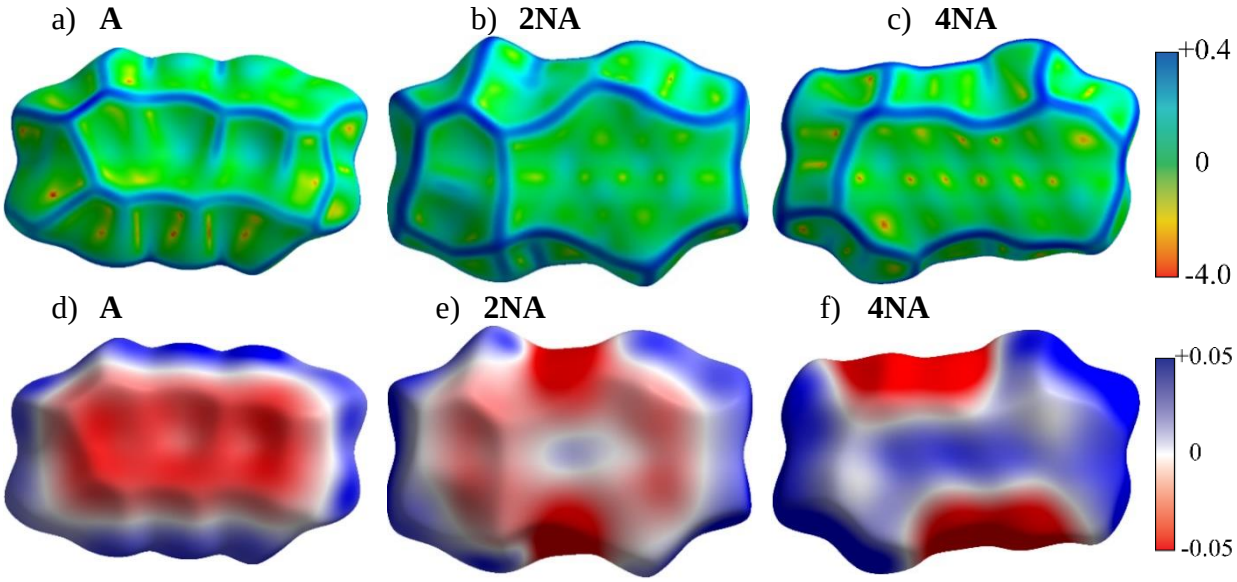

Figure 5. Hirshfeld surfaces of **A**, **2NA** and **4NA** mapped with curvedness (a-c) and ESP (±65.6 kJ mol^{-1} per unit charge) (d-f)).

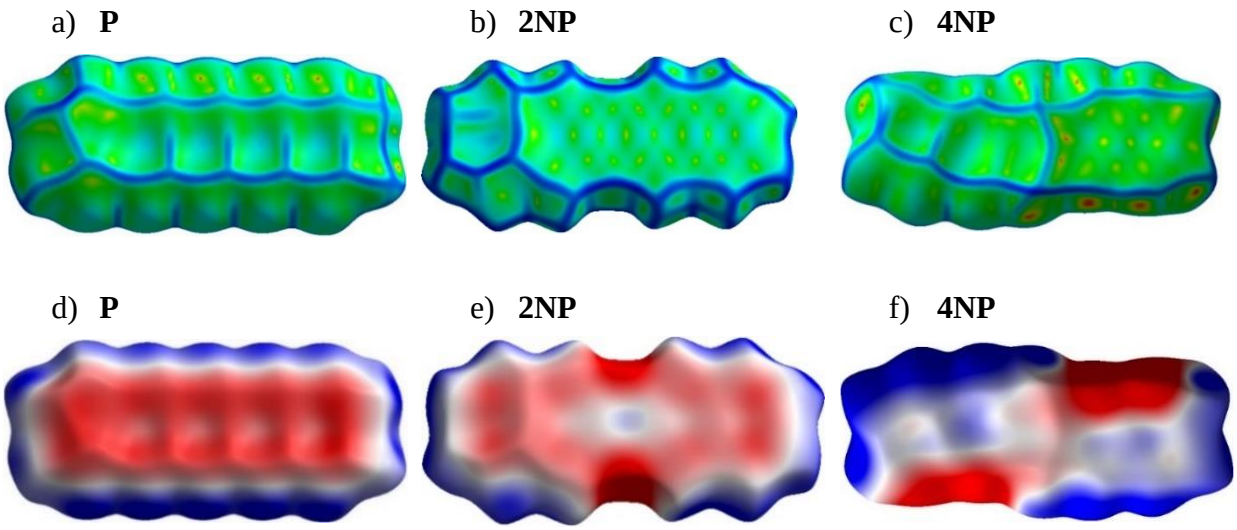

Figure 6. Hirshfeld surfaces of **P**, **2NP** and **4NP** mapped with curvedness C (a-c) and ESP (±65.6 kJ mol^{-1} per unit charge) (d-f)). Color scheme corresponds to Figure 5.

Figure 7 presents the distribution of the intermolecular contacts by the atom type for **A** and **P** series. From Figure 7a it follows that in **A**, most contacts are either C···H or H···H, which is a common feature of the herringbone packing. These contacts are not favorable for charge transport

Preprints (www.preprints.org) | NOT PEER-REVIEWED | Posted: 8 July 2020 doi:10.20944/preprints202007.0149.v1

Peer-reviewed version available at Int. J. Mol. Sci. 2020, 21, 5654; doi:10.3390/ijms21165654

("insulating") since hydrogen atoms bear negligible electron density on the frontier orbitals (HOMO and LUMO). On the contrary, in **2NA** and **4NA**, the contacts between non-hydrogen atoms, namely C···C and C···N ones, emerge, and their contribution increases with the number of nitrogen atoms in the molecule (see also Figure S5). These findings are in line with the results of previous studies for slightly N-substituted azaacenes [23, 24]. C···C and C···N contacts are favorable for charge transport ("conductive") since they enable larger *J* values due to the efficient overlap between the frontier orbitals of the adjacent molecules: both the C and N atoms can bear considerable π-electron (HOMO and/or LUMO) density. The increase in the number of "conductive" contacts with N-substitution is also observed for pentacene (Figure 7b and S10) and tetracene (Figure S7) series. Interestingly, in the azaacenes with four nitrogen atoms, N···N contacts (which should be electrostatically unfavorable, see Figure S11) are observed. We assume that these contacts are an unintentional byproduct of the stronger attractive CH···N interactions: energy decrease due to the latter contacts probably overwhelm energy increase caused by N···N electrostatic repulsion. Note that azaacenes with more than two nitrogen atoms and hence extended electron-deficient and -rich areas were not addressed theoretically before, so the effect of such heavy N-substitution on crystal packing and charge-transport observed herein is more pronounced than that was previously reported in Refs. [23-25].

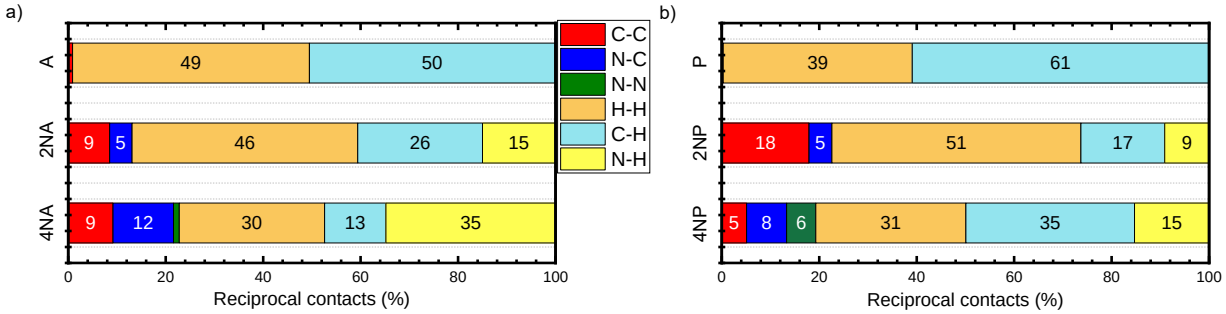

Figure 7. Distribution of reciprocal intermolecular contacts for selected compounds from **A** (a) and **P** (b) series arranged by molecules. "Conductive" contacts are shown in red, blue and green.

Charge transport

To monitor the changes in the electron and hole mobilities with N-substitution, we applied hopping model of charge transport based on the Marcus formula for charge transfer ("hop") rate [43]:

$$k = \frac{2\pi}{\hbar} J^2 \left(\frac{1}{4\pi\lambda k_B T} \right)^{1/2} \exp\left(-\frac{(\Delta E - \lambda)^2}{4\lambda k_B T} \right), \quad (1)$$

where ħ is the reduced Planck constant, k_B is the Boltzmann constant, T is the absolute temperature, and ΔE is the electron energy difference between the initial and final sites (ΔE=0 for identical molecules). Then, the charge-carrier (hole or electron) diffusion coefficient was calculated by summation over all the transport directions, i.e. all the pairs of the given molecule with its neighbors, and finally isotropic hole and electron mobilities, μ_h and μ_e, were calculated using the Einstein–Smoluchowski relation (see details in SI, Section S4). As follows from Eq. (1), *J* and λ are the main parameters determining the charge transport within the hopping model. As mentioned above, the former is associated with the electronic interaction between the molecules, while the latter is determined by the electron-vibrational interaction. We will first analyze the impact of N-substitution on these parameters and then turn to its impact on μ.

Preprints (www.preprints.org) | NOT PEER-REVIEWED | Posted: 8 July 2020 doi:10.20944/preprints202007.0149.v1

Peer-reviewed version available at Int. J. Mol. Sci. 2020, 21, 5654; doi:10.3390/ijms21165654

Reorganization energies

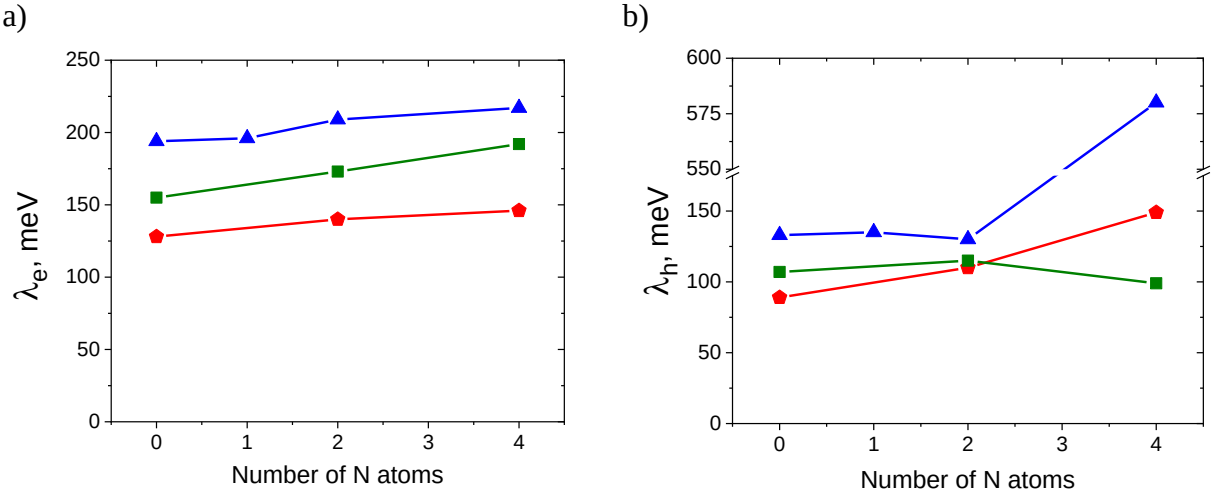

Figure 8. Electron (a) and hole (b) transfer reorganization energies for the compounds studied.

Figure 8 presents the calculated reorganization energies for oligoacenes and their N-substituted counterparts. As follows from Figure 8a, reorganization energy for electron transport, λ_e, increases with N-substitution. This is in line with previous results for azapentacenes [12] and could be attributed to the decrease of the non-bonding character of LUMO in N-substituted oligoacenes [44] and decreased aromaticity [45]. However, the increase is rather small (less than 25%), and is not expected to reduce the charge mobility dramatically. The small changes in λ_e with N-substitution can be attributed to the small impact of the latter on the LUMO pattern. Indeed, similar LUMO pattern of oligoacenes and azaacenes should result in similar electron-vibrational interaction, i.e. similar λ_e, since molecular vibrations are not expected to be strongly altered with N-substitution due to comparable atomic masses of CH group and N atom and comparable energies of C=C and C=N bonds. Noteworthily, the small increase is probably related to the symmetric character of N-substitution: asymmetric N-pentacenes show much larger λ_e [12], probably due to the significant changes in the LUMO pattern as a result of asymmetric insertion of heteroatoms.

Reorganization energies for hole transfer show a more complicated behavior with N-substitution as shown in Figure 8b. For **4NA**, λ_h is more than twice as large as that for the other anthracene derivatives studied and amounts ~580 meV (note that change of the DFT functional from B3LYP to PBE resulted in similar λ_h ~ 520 meV). Such a high λ_h can be attributed to the qualitatively different HOMO pattern in **4NA** molecule than in the other OSs studied (see Figure S1): this pattern nearly lacks any nodes on the bonds, in contrast to that of the other compounds studied. On the contrary, λ_h for **2NA** is lower than that for the other members of **A** series, which can be attributed to the stronger non-bonding character of HOMO (more pronounced nodes on the bonds) in this compound. Indeed, the larger the number of HOMO nodes on the bonds, the weaker the hole-vibrational interaction, i.e. the lower the λ_h [46].

Figure 9 shows how the contributions of various vibrational modes to λ_e change with N-substitution and compares these changes with the changes in the Raman spectrum, which was suggested to monitor the electron-vibrational interaction [47-49]. From this figure it follows that the main contribution to λ_e stems from two collective modes shown in Figure 7c,d: the conjugated skeleton stretching along the molecular long-axis (mode 1) and the collective C=C stretching vibrations and C–H wagging vibrations (mode 2), in line with Ref. [25]. These vibrations distort the bonds where LUMO is localized, resulting in strong electron-vibrational coupling (cf. Figures 2 and 9c,d). With N-substitution, the frequency of the mode 1 slightly increases, and that of mode 2 decreases, in line with Ref. [25]. The contribution of the latter mode to λ increases significantly, while that of the former decreases.

It was shown in Ref. [47] that for a particular class of organic semiconductors – charge transfer complexes – the contribution of the vibrational mode to the reorganization energy is

Preprints (www.preprints.org) | NOT PEER-REVIEWED | Posted: 8 July 2020 doi:10.20944/preprints202007.0149.v1

Peer-reviewed version available at Int. J. Mol. Sci. 2020, 21, 5654; doi:10.3390/ijms21165654

related to its Raman intensity: $\lambda_i \propto I_i/\omega_i$, where ω_i is the frequency of the mode. Although the correlation between I_i/ω_i and λ_i was observed for few single-component OSs as well [48, 49], generalization of this relation to the other OSs is lacking. From Figure 9b it follows that for both **P** and **4NP**, the modes 1 and 2, which show the largest λ_i, also have the largest I_i/ω_i ratio, and changes in this ratio with N-substitution (significant increase for mode 2) resembles the changes in λ_i. Moreover, from Figure 9 it follows that changes in the total λ_e between **P** and **4NP** correlate with the changes in spectrally integrated I_i/ω_i: the both quantities increase with N-substitution. Thus, our findings highlight the potential of Raman spectroscopy for monitoring the changes in the electron-vibrational interaction with subtle changes in the chemical structure, e.g. N-substitution; however, this is a subject of a separate study.

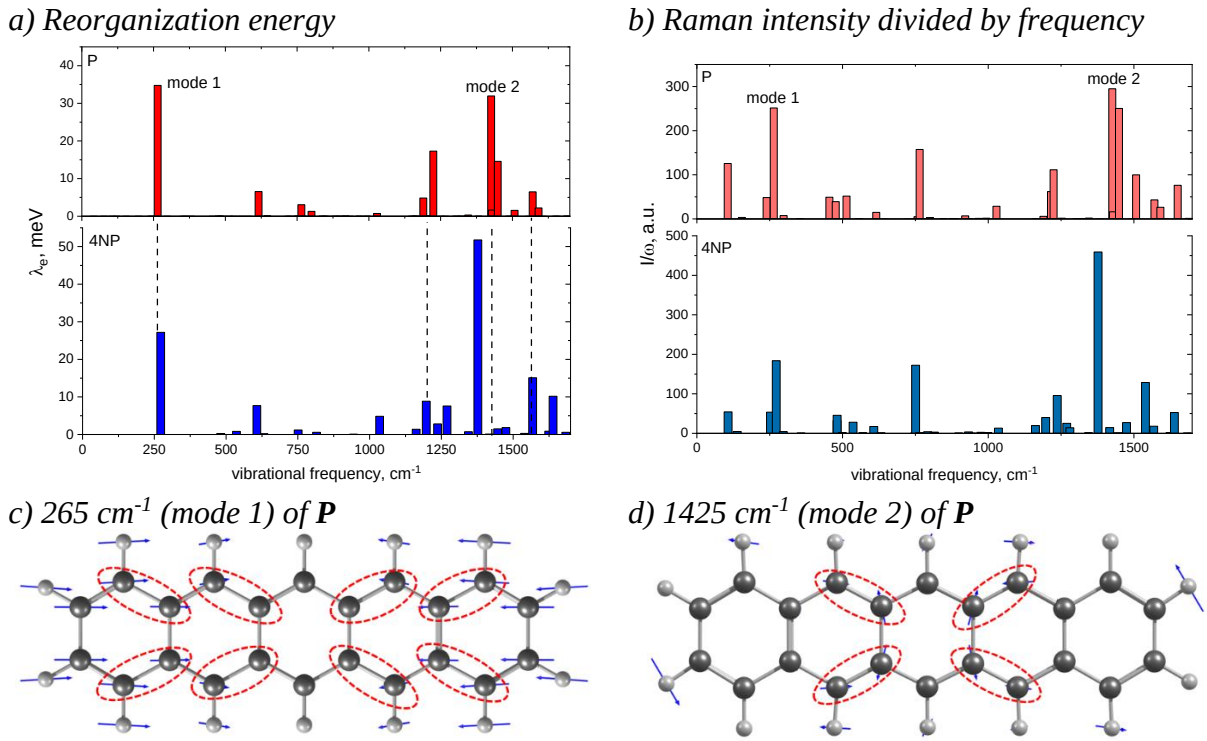

Figure 9. (a,b) Contribution of various vibrational modes to the electron transfer reorganization energy, λ_i (a), and Raman intensities of these modes divided by their frequency, I_i/ω_i (b), for **P** (top) and **4NP** (bottom). (c,d) Vibrational displacements for the modes showing the largest contribution to λ and I/ω (labeled "mode 1" and "mode 2" in panels (a,b)). Dashed ellipses highlight bonds with considerable LUMO density (see Figure 2) that are significantly modulated by the corresponding vibrations.

Charge transfer integrals

Figure 10 shows the hole and electron transfer integrals for **A**, **P** and their selected N-substituted derivatives. From this Figure it follows that for **A** and **P** series, N-substitution generally results in the crossover from three directions of moderate charge transport to single direction with efficient charge transport – direction of face-to-face molecular arrangement (π-stacking, see Figure S13) – for both holes and electrons. This is natural since face-to-face interactions are stabilized by N-substitution in the crystals studied, and π-stacking is facilitated. Moreover, similar changes in the charge transport dimensionality were observed in Ref. [19], where variations in the molecular electrostatic potential with partial fluorination induced crossover to π-stacking packing motif and (quasi) one-dimensional charge transport. Noteworthily, completely one-dimensional charge transport is generally detrimental for μ [1, 2, 9, 50]; however, in **4NA** and **4NP**, J_e (and also J_h for the former compound) in the other directions amount ~20 meV making the charge transport not completely one-dimensional but quasi-one-dimensional. The latter regime seems to be compatible

Preprints (www.preprints.org) | NOT PEER-REVIEWED | Posted: 8 July 2020 doi:10.20944/preprints202007.0149.v1

Peer-reviewed version available at Int. J. Mol. Sci. 2020, 21, 5654; doi:10.3390/ijms21165654

with high μ: for instance, in one of the most efficient p-type OSs, rubrene [2], and decent n-type OS TCNQ [9], large J is also observed in one direction, and J values for the other directions amount ~20 meV [8]. Noteworthily, as follows from Figure 10, the largest J for studied N-substituted anthracenes and pentacenes (except for **2NA**) are larger than those for the non-substituted counterparts. For **4NT**, all J are small – there is only one direction with J_h=45 meV and J_e=13 meV, – which indicates poor matching of the frontier orbitals' phases for adjacent molecules despite of their considerable spatial overlap, presumably because of poor ESP complementarity.

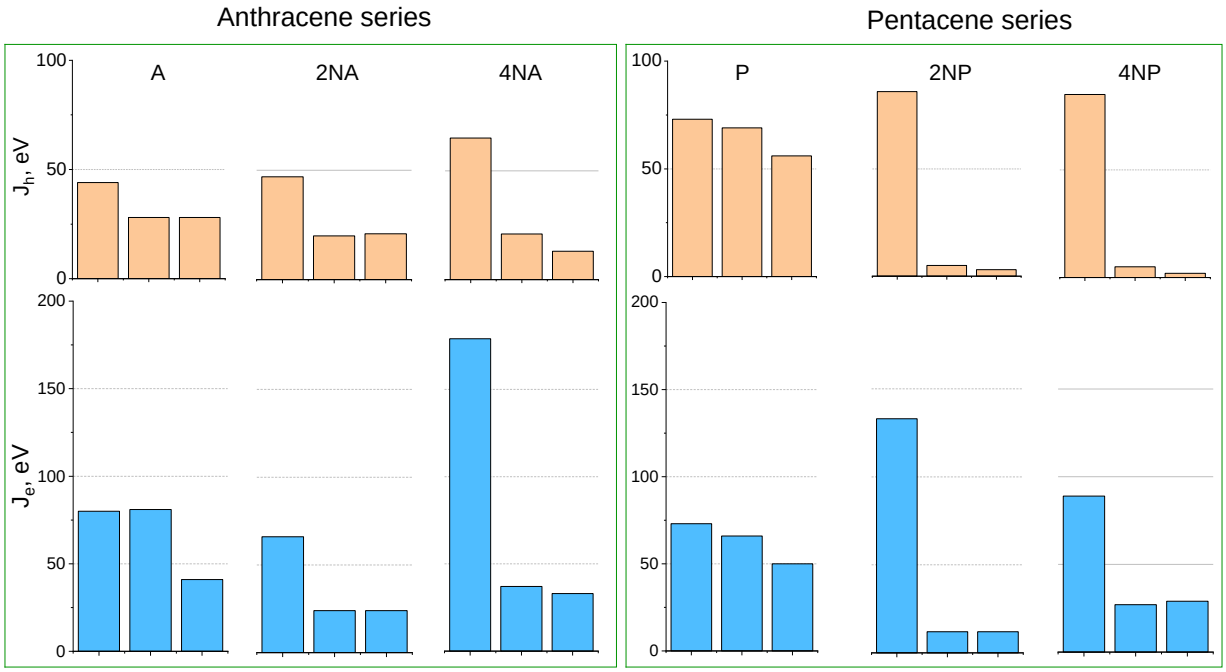

Figure 10. Hole (top, J_h) and electron (bottom, J_e) transfer integrals for the selected crystals from (aza)anthracene and (aza)pentacene series. For each crystal, three largest $J_{h,e}$ for different directions are shown.

Charge mobilities

Figure 11 collates the calculated hole and electron mobilities for the compounds studied. The hole mobility slightly increases as a result of insertion of two nitrogen atoms for **T** and **P** series, yielding μ_h~1.8 and 2.3 $cm^2V^{-1}s^{-1}$ for **2NT** and **2NP**, respectively, but remains nearly unaffected for **2NA** (μ_h~*0.4* $cm^2V^{-1}s^{-1}$). Further N-substitution has even more discrepant effect on μ_h. Specifically, for **4NP**, μ_h significantly exceeds that for **P** amounting remarkably high ~4.3 $cm^2V^{-1}s^{-1}$. So high μ_h can be attributed to large J_h (see Figure 10), decent λ_h (see Figure 8) and significant slip of the molecules along the long molecular axis resulting in large distance between the molecular centers, r, in the in the direction of the most efficient transport (r~9 Å for **4NP** vs r~4 Å for **4NP**). The latter is beneficial for the charge transport since the larger the hopping distance, the larger the μ (see Eqs. (S1-S2)). For **4NA** and **4NT**, μ_h is lower than for **A** and **T**, respectively. Low μ_h for **4NA** can be attributed to the extremely high λ_h for this compound (see Figure 8), while low μ_h for **4NT** can be explained by small J_h.

Electron mobility decreases as a result of insertion of two nitrogen atoms in the central ring for both the **2NA** and **2NT**, but increases for **2NP**, as compared to the non-substituted counterparts. As a result, in **2NP** μ_e exceeds 3 $cm^2V^{-1}s^{-1}$. Four nitrogen atoms result in the increase of the electron mobility for **4NA** and **4NP** yielding μ_e~1.3 and ~3.6 $cm^2V^{-1}s^{-1}$, respectively. High μ_e in the former OS can be attributed to very large J_e~175 meV (see Figure 10), which significantly exceed the typical values for high-mobility OSs [2]. For **4NP**, high μ_e can be explained by decent J_e~85 meV, the abovementioned slip of the molecules along the long molecular axis and moderate λ_e (see Figure 8). Noteworthily, our results were obtained within Marcus model, which typically

Preprints (www.preprints.org) | NOT PEER-REVIEWED | Posted: 8 July 2020 doi:10.20944/preprints202007.0149.v1

Peer-reviewed version available at Int. J. Mol. Sci. 2020, 21, 5654; doi:10.3390/ijms21165654

underestimates μ. Furthermore, our μ_e estimate for **4NP** is larger than that we obtained at similar conditions for TIPS-TAP (2.7 $cm^2V^{-1}s^{-1}$) – the TIPS-substituted tetraazapentacene with high experimental μ_e = 3.3 $cm^2V^{-1}s^{-1}$ [26].

For operation of OFETs and other electronic devices, not just high μ is required, but also efficient charge injection [51]. As follows from Figure 3, HOMO and LUMO levels are lowered with N-substitution, and hence, electron injection becomes more favorable, while hole injection becomes less favorable. This is in line with experimental data [26]: while pentacene and **2NP** showed hole (p-type) conductivity in OFETs, **4NP** (isomer of the compound studied herein) exhibited electron (n-type) conductivity. Since LUMO levels of **4NA** and **4NT** are close to that of **4NP**, we expect that these compounds can also show electron conductivity. In conjunction with high predicted electron mobility (see Figure 9), they are promising for application in n-type OFETs. **2NT** and **2NP** could show efficient hole injection and transport and outperform **T** and **P** in p-type OFETs, respectively. Finally, **2NP** and **4NP** could probably yield ambipolar mobility.

Thus, azaacenes without side groups can show very high μ_h and μ_e. Lack of high experimental μ data for these materials can be caused by the polycrystalline nature of their thin films studied in OFETs or their low HOMO/high LUMO levels (as compared, e.g., with non-substituted acenes [2] and TIPS-substituted counterparts [26]). These factors could result in the increased number of defects due to lower oxidation stability [52]. Moreover, synthesis of **4NA** was reported very recently [53], and this compound was probably not tested in organic electronic devices.

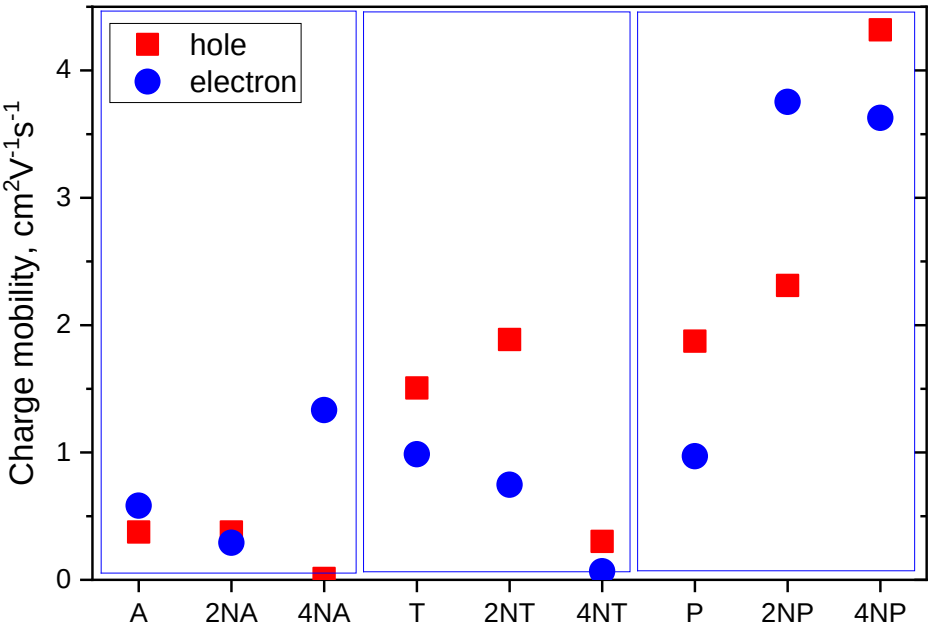

Figure 11. Calculated charge mobilities for the compounds studied.

Discussion

Our results highlight dramatic impact of N-substitution on the crystal structure of linear oligoacenes. This is in line with previous observations [13,14,23,25] and extends the results of the mentioned studies towards heavily N-substituted (bearing four nitrogen atoms) oligoacenes. Specifically, N-substitution facilitates π-stacking and increases the number of "conductive" C···C and C···N (and sometimes N···N) intermolecular contacts instead of "insulating" H···H and C···H contacts, which dominate in oligoacenes. These structural changes can result in the increase of J, in line with previous observations for N-substituted oligoarenes [54]. Within the studied series of anthracene, tetracene and pentacene derivatives, J and r_i values determine the charge mobilities, while λ remain comparable (except for the case of hole transport in **4NA**, see Figure 8).

Surprisingly, our results show that facilitated π-stacking does not necessarily increase charge mobility (cf. Figures 5-7 and 11). Nevertheless, **4NA** and **4NP** – compounds where N-

Preprints (www.preprints.org) | NOT PEER-REVIEWED | Posted: 8 July 2020 doi:10.20944/preprints202007.0149.v1

Peer-reviewed version available at Int. J. Mol. Sci. 2020, 21, 5654; doi:10.3390/ijms21165654

substitution is heavy and its pattern has center of symmetry but lacks plane of symmetry – show either the largest electron or the largest hole mobilities in the **A** and **P** series, respectively. We suggest that this is because such symmetry of N-substitution results in pronounced and large electron-rich and electron-deficient "stripes", which facilitate efficient π-stacking and favorable HOMO and/or LUMO overlap. **4NT**, where the pattern of N-substitution has both the center and the plane of symmetry, shows low μ_e and μ_h due to small *J*, probably dictated by the mismatch of the HOMO and LUMO phases. Thus, we suggest that molecules with considerable ratio of nitrogen atoms in the conjugated core, the substitution pattern with center of symmetry but lacking plane of symmetry, and large electron-rich/electron-deficient areas are promising for efficient charge transport.

Finally, from the analysis provided herein, an interesting conclusion can be derived that goes beyond the frames of conventional organic electronics. Specifically, nitrogen-containing aromatic compounds are widely spread in the nature. For instance, nucleobases – the π-conjugated cores of the DNA and RNA monomer units – involve either purine or pyrimidine N-heterocycles. Multiple nitrogen heteroatoms in the nucleobases make ESP of these compounds non-uniform, with pronounced areas of positive and negative charge (see Figure 12). As a result, molecular packing for the crystalline nucleobases shows significant amount of π-stacking like for azaacenes addressed in this study. Indeed, as shown in Figure 12 for uracil and adenine, the Hirshfeld surfaces mapped with curvedness show flat green areas associated with π-stacking, in line with our conclusions for azaacenes (see Figure 3). Charge transfer integrals for these crystals (which are actually wide-gap OSs [55]) are also rather large (up to 97 meV, see Table S2). We suggest that large *J* in these crystals stem from the favorable arrangement of the molecules due to the electrostatic interaction between the electron-rich and electron-deficient areas (ESP complementarity). These findings can be useful for the search and/or design of the natural or nature-inspired OSs and can improve our understanding of the charge transport in biomolecules, e.g. nucleic acids, which gained particular attention in the last decade due to its key role in bioprocesses [56, 57]. A more detailed analysis of the intermolecular interactions and structure-property relationships in the assemblies of nucleobases is a subject of our ongoing study.

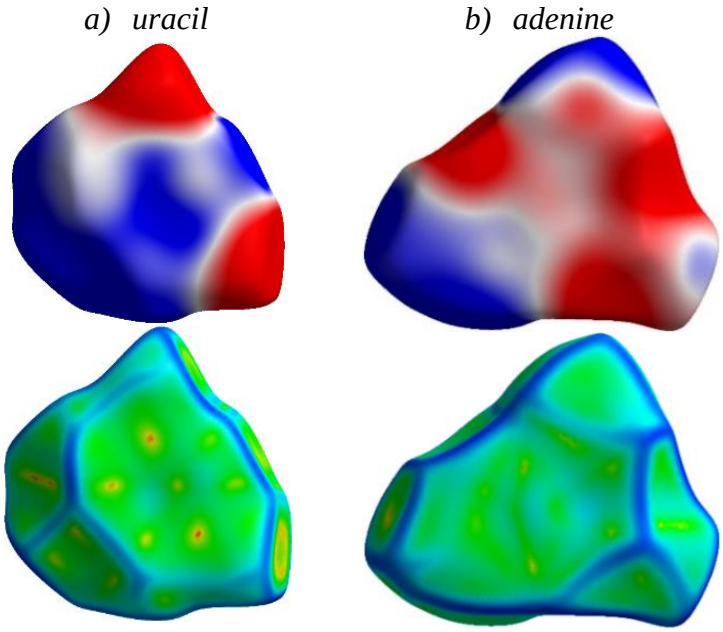

Figure 12. Hirshfeld surfaces for uracil (a) and adenine (b) crystals mapped with ESP (top) and curvedness (bottom). Details for color scheme are given in Figure 5.

Conclusions

We have analyzed computationally the effect of up to four nitrogen atoms insertion (N-substitution) into the π-conjugated cores of anthracene, tetracene and pentacene. The relationship between the molecular structure, molecular properties, crystal structure and charge mobility was

in the focus of the study. It has been found that N-substitution facilitates π-stacking molecular arrangement in the corresponding crystals that generally result in large charge transfer integrals favorable for charge transport. The changes in the molecular packing have been attributed to the dramatic changes in the molecular electrostatic potential, in line with earlier studies for lightly N-substituted acenes. Hole and electron mobilities in the crystals of various azaacenes have been calculated for the first time, and their values exceeded 1 $cm^2V^{-1}s^{-1}$ for several compounds. Importantly, azaacenes with four nitrogen atoms forming pronounced electron-rich and electron-deficient areas arranged in a pattern with center of symmetry but without plane of symmetry have shown either the largest electron or the largest hole mobilities in their series. Finally, we have extrapolated our conclusions on the nucleobases – natural compounds bearing multiple nitrogen atoms in their conjugated cores. Our results highlight that smart tuning of the molecular electrostatic potential can be an efficient tool in designing of the organic semiconducting crystals for steady improvement of the organic electronics.

Acknowledgements

We thank Prof. Q. Miao for providing crystal structure of diazapentacene (2NP) and D. Yu. Paraschuk for fruitful discussions. Charge mobility calculations were supported by Russian Foundation for Basic Research (project # 19-32-60081) and performed in the Institute of Biochemistry. Studies on the vibrational decomposition of the reorganization energies and calculation of the Raman spectra were supported by Russian Science Foundation (project # 18-72-10165) and performed in the Institute of Spectroscopy. Theoretical analysis of the crystal structures was performed with the support from the Foundation for the advancement of theoretical physics and mathematics «BASIS» in the Lomonosov Moscow State University.

Conflicts of interest

There are no conflicts to declare.

Author Contributions

Conceptualization, Andrey Sosorev; Investigation, Andrey Sosorev, Dmitry Dominskiy and Ivan Chernyshov; Project administration, Andrey Sosorev; Supervision, Andrey Sosorev; Visualization, Dmitry Dominskiy; Writing – original draft, Andrey Sosorev, Dmitry Dominskiy, Ivan Chernyshov and Roman Efremov.

References

1. G. Schweicher, G. Garbay, R. Jouclas, F. Vibert, F. Devaux, Y. H. Geerts. Molecular Semiconductors for Logic Operations: Dead-End or Bright Future? Adv. Mater. 2020, 1905909.
2. O. Ostroverkhova, Organic Optoelectronic Materials: Mechanisms and Applications, Chem. Rev. 2016, 116, 13279-13412.
3. T. Akasaka, A. Osuka, S. Fukuzumi, H. Kandori, Y. Aso, Chemical Science of π-Electron Systems, Springer Japan, 2015.
4. G. Schweicher, Y. Olivier, V. Lemaur, Y. H. Geerts. What Currently Limits Charge Carrier Mobility in Crystals of Molecular Semiconductors? Isr. J. Chem. 2014, 54, 595-620.
5. A. Troisi. Charge transport in high mobility molecular semiconductors: classical models and new theories. Chem. Soc. Rev. 2011, 40, 2347–2358.
6. A. Köhler, H. Bässler, Electronic Processes in Organic Semiconductors: an Introduction. Wiley-VCH, Weinheim, 2015.
7. Y. Li, V. Coropceanu, J.-L. Brédas, in The WSPC Reference on Organic Electronics: Organic Semiconductors, ed. J.-L. Brédas, S. R. Marder, World Scientific, Singapore, 2016. Chapter 7, 193

8. A. Yu. Sosorev. Simple charge transport model for efficient search of high-mobility organic semiconductor crystals, Mater. Des. 2020, 192, 108730.
9. A. Yu. Sosorev. Role of intermolecular charge delocalization and its dimensionality in efficient band-like electron transport in crystalline 2,5-difluoro-7,7,8,8-tetracyanoquinodimethane (F_2-TCNQ), Phys. Chem. Chem. Phys. 2017, 19, 25478-25486.
10. V. Coropceanu, J. Cornil, D. A. da Silva Filho, Y. Olivier, R. Silbey, J.-L. Brédas, Charge Transport in Organic Semiconductors. Chem. Rev. 2007, 107, 926.
11. M. K. Corpinot, D.-K. Bučar. A Practical Guide to the Design of Molecular Crystals. Cryst. Growth Des. 2019, 19, 1426−1453.
12. H.-Y. Chen, I. Chao. Toward the Rational Design of Functionalized Pentacenes: Reduction of the Impact of Functionalization on the Reorganization Energy. Chem. Phys. Chem. 2006, 7, 2003-2007
13. J. E. Campbell, J. Yang, G. M. Day. Predicted energy–structure–function maps for the evaluation of small molecule organic semiconductors J. Mater. Chem. C 2017, 5, 7574.
14. M. Klues, G. Witte. Crystalline packing in pentacene-like organic semiconductors. CrystEngComm 2018, 20, 63.
15. I. Yu. Chernyshov, M. V. Vener, E. V. Feldman, D. Yu. Paraschuk, A. Yu. Sosorev. Inhibiting low-frequency vibrations explains exceptionally high electron mobility in 2,5-difluoro-7,7,8,8-tetracyanoquinodimethane (F_2-TCNQ) single crystals. J. Phys. Chem. Lett. 2017, 8, 2875–2880.
16. P. Kirsch, Q. Tong, H. Untenecker. Crystal design using multipolar electrostatic interactions: A concept study for organic electronics. Beilstein J. Org. Chem. 2013, 9, 2367–2373.
17. C. Wang, H. Dong, W. Hu, Y. Liu, D. Zhu Semiconducting π-Conjugated Systems in Field-Effect Transistors: A Material Odyssey of Organic Electronics. Chem. Rev. 2012, 112, 2208–2267.
18. Y.-C. Chang, Y.-D. Chen, C.-H. Chen, Y.-S. Wen, J. T. Lin, H.-Y. Chen, M.-Y. Kuo, I. Chao Crystal Engineering for π-π Stacking via Interaction between Electron-Rich and Electron-Deficient Heteroaromatics. J. Org. Chem. 2008, 73, 4608–4614.
19. J.-H. Dou, Y.-Q. Zheng, Z.-F. Yao, Z.-A. Yu, T. Lei, X. Shen, X.-Y. Luo, J. Sun, S.-D. Zhang, Y.-F. Ding, G. Han, Y. Yi, J.-Y. Wang, J. Pei. Fine-Tuning of Crystal Packing and Charge Transport Properties of BDOPV Derivatives through Fluorine Substitution. J. Am. Chem. Soc. 2015, 137, 15947−15956.
20. E. Menard, V. Podzorov, S. H. Hur, A. Gaur, M. E. Gershenson, J. A. Rogers. High-Performance n- and p-Type Single-Crystal Organic Transistors with Free-Space Gate Dielectrics. Adv. Mater. 2004, 16, 2097-2101.
21. Y. Krupskaya, M. Gibertini, N. Marzari, A. F. Morpurgo. Band-like electron transport with record-high mobility in the TCNQ family. Adv. Mater. 2015, 27, 2453-2458.
22. E. Komissarova, D. Dominsky, V. Zhulanov, G. G. Abashev, S. Afzal, S. P. Singh, A. Yu. Sosorev, D. Yu. Paraschuk. Unraveling the unusual effect of fluorination on crystal packing in organic semiconductor. Phys. Chem. Chem. Phys. 2020, 22, 1665-1673.
23. P.-P. Lin, G.-Y. Qin, N.-X. Zhang, J.-X. Fan, X.-L. Hao, L.-Y. Zou, A.-M. Ren. The roles of heteroatoms and substituents on the molecular packing motif from herringbone to π-stacking: A theoretical study on electronic structures and intermolecular interaction of pentacene derivatives. Organic Electronics 2020, 78, 105606.
24. K. E. Maly. Acenes vs N-Heteroacenes: The Effect of N-Substitution on the Structural Features of Crystals of Polycyclic Aromatic Hydrocarbons. Cryst. Growth Des. 2011, 11, 12, 5628–5633
25. X.-K. Chen, J.-F. Guo, L.-Y. Zou, A.-M. Ren, J.-X. Fan. A Promising Approach to Obtain Excellent n-Type OrganicField-Effect Transistors — Introducing Pyrazine Ring. J. Phys. Chem. C 2011, 115, 43, 21416–21428.
26. Q. Miao. Ten Years of N-Heteropentacenes as Semiconductors for Organic Thin-Film Transistors. Adv. Mater. 2014, 26, 5541–5549.

27. E. F. Valeev, V. Coropceanu, D. A. da Silva Filho, S. Salman, J.-L. Bredas. Effect of Electronic Polarization on Charge-Transport Parameters in Molecular Organic Semiconductors. J. Am. Chem. Soc. 2006, 128, 9882.

28. C. Reese, W.-J. Chung, M.-M. Ling, M. Roberts, Z. Bao. High-performance microscale single-crystal transistors by lithography on an elastomer dielectric Appl. Phys. Lett. 2006, 89, 202108.

29. J.-L. Brédas, S. R. Marder, J.-M. André, in The WSPC Reference on Organic Electronics: Organic Semiconductors, ed. J.-L. Brédas, S. R. Marder, World Scientific, Singapore, 2016, Chapter 1, 1.

30. M. Winkler and K. Houk. Nitrogen-Rich Oligoacenes: Candidates for n-Channel Organic Semiconductors. J. Am. Chem. Soc. 2007, 129, 1805.

31. A. L. Appleton, S. M. Brombosz, S. Barlow, J. S. Sears, J.-L. Brédas, S. R. Marder, U. H.F. Bunz. Effects of electronegative substitution on the optical and electronic properties of acenes and diazaacenes. Nat. Commun., 1, 91

32. M. W. Schmidt, K. K. Baldridge, J. A. Boatz, S. T. Elbert, M. S. Gordon, J. H. Jensen, S. Koseki, N. Matsunaga, K. A. Nguyen, S. Su, T. L. Windus, M. Dupuis, J. A. Montgomery. General atomic and molecular electronic structure system, J. Comput. Chem. 1993, 14, 1347-1363.

33. M. S. Gordon, M.W. Schmidt. Advances in Electronic Structure Theory: GAMESS a Decade Later. In Theory and Applications of Computational Chemistry: the first forty years, ed. C. E. Dykstra, G. Frenking, K. S. Kim, G. E. Scuseria, Elsevier, Amsterdam, 2005, p. 1167-1189.

34. A. Yu. Sosorev, I. Yu. Chernyshov, D. Yu. Paraschuk, M. V. Vener. Intra- and Intermolecular Vibrations of Organic Semiconductors and Their Role in Charge Transport. In Molecular Spectroscopy (eds Y. Ozaki, M. J. Wójcik and J. Popp), chapter 15. Wiley, 2019

35. B. Baumeier, J. Kirkpatrick and D. Andrienko, Density-functional based determination of intermolecular charge transfer properties for large-scale morphologies. Phys. Chem. Chem. Phys. 2010, 12, 11103.

36. J. Kirkpatrick, An Approximate Method for Calculating Transfer Integrals Based on the ZINDO Hamiltonian. Int. J. Quantum Chem., 2008, 108, 51.

37. H. Kobayashi, N. Kobayashi, S. Hosoi, N. Koshitani, D. Murakami, R. Shirasawa, Y. Kudo, D. Hobara, Y. Tokita and M. Itabashi, Hopping and band mobilities of pentacene, rubrene, and 2,7-dioctyl[1]benzothieno[3,2-b][1]benzothiophene (C8-BTBT) from first principle calculations. J. Chem. Phys. 2013, 139, 8.

38. M. J. Turner, J. J. McKinnon, S. K. Wolff, D. J. Grimwood, P. R. Spackman, D. Jayatilaka, M. A. Spackman, CrystalExplorer17, University of Western Australia, 2017, http:// hirshfeldsurface.net.

39. C. F. Mackenzie, P. R. Spackman, D. Jayatilaka, M. A. Spackman. CrystalExplorer model energies and energy frameworks: extension to metal coordination compounds, organic salts, solvates and open-shell systems. IUCrJ 2017, 4, 575

40. J. Dhar, U. Salzner, S. Patil. Trends in molecular design strategies for ambient stable n-channel organic field effect transistors. J. Mater. Chem. C, 2017, 5, 7404

41. J. J. McKinnon, M. A. Spackman, A. S. Mitchell. Novel Tools for Visualizing and Exploring Intermolecular Interactions in Molecular Crystals. Acta Crystallogr., Sect. B 2004, 60, 627−668.

42. M. A. Spackman, P. G. Byrom. A novel definition of a molecule in a crystal. Chem. Phys. Lett. 1997, 267, 215.

43. R.A. Marcus, N. Sutin. Electron transfers in chemistry and biology, Biochim. Biophys. Acta 1985, 811, 265-322.

44. T. Kato and T. Yamabe, Electron−Phonon Interactions in the Monoanions of Polycyanodienes. J. Phys. Chem. A 2004, 108, 11223-11233.

45. S. Gümüş, M. Akbay. A Computational Study on Substituted and Unsubstituted Mono and Diazaanthracenes. Polycyclic Aromatic Compounds 2013, 33, 519–532

46. W.-C. Chen, I. Chao. Molecular Orbital-Based Design of π-Conjugated Organic Materials with Small Internal Reorganization Energy: Generation of Nonbonding Character in Frontier Orbitals J. Phys. Chem. C 2014, 118, 20176−20183

47. A. B. Myers, Resonance Raman Intensities and Charge-Transfer Reorganization Energies, Chem. Rev. 1996, 96, 911–926.

48. A. Yu. Sosorev. The Electron-Vibrational Interaction in a Thiophene—Phenylene Co-oligomer and Its Relationship to the Raman Spectrum. Moscow University Physics Bulletin, 2019, 74, 639–645.

49. R. Scholz, L. Gisslén, C. Himcinschi, I. Vragović, E. M. Calzado, E. Louis, E. San Fabián Maroto and M. A. Díaz-García, Asymmetry between Absorption and Photoluminescence Line Shapes of TPD: Spectroscopic Fingerprint of the Twisted Biphenyl Core. J. Phys. Chem. A 2009, 113, 315.

50. J. Roncali, P. Leriche, A. Cravino. From One- to Three-Dimensional Organic Semiconductors: In Search of the Organic Silicon. Adv. Mater. 2007, 19, 2045–2060

51. A. Yu. Sosorev, V. A. Trukhanov, D. R. Maslennikov, O. V. Borshchev, R. A. Polyakov, M. S. Skorotetcky, N. M. Surin, M. S. Kazantsev, D. I. Dominskiy, V. A. Tafeenko, S. A. Ponomarenko, D. Yu. Paraschuk, Fluorinated Thiophene-Phenylene Co-Oligomers for Optoelectronic Devices, ACS Appl. Mater. Interfaces. 2020, 12, 9507-9519

52. N. B. Kotadiya, A. Mondal, P. W. M. Blom, D. Andrienko, G.-J. A. H. Wetzelaer. A window to trap-free charge transport in organic semiconducting thin films. Nat. Mater. 2019, 18, 1182–1186

53. N. Ukwitegetse, P. J. G. Saris, J. R. Sommer, R. M. Haiges, P. I. Djurovich, M. E. Thompson. Tetra-Aza-Pentacenes by means of a One-Pot Friedländer Synthesis Chem. Eur. J. 2019, 25, 1472.

54. V. A. Trukhanov, D. I. Dominskiy, O. D. Parashchuk, E. V. Feldman, N. M. Surin, E. A. Svidchenko, M. S. Skorotetcky, O. V. Borshchev, D. Yu. Paraschuk, A. Yu. Sosorev. Exploring the impact of N-substitution on structural, electronic, optical and vibrational properties of thiophene-phenylene co-oligomer. Submitted to RSC Adv. 2020.

55. F. F. Maia Jr., V. N. Freire, E. W. S. Caetano, D. L. Azevedo, F. A. M. Sales, E. L. Albuquerque. Anhydrous crystals of DNA bases are wide gap semiconductors. J. Chem. Phys. 2011, 134, 175101.

56. E. O'Brien, M. E. Holt, M. K. Thompson, L. E. Salay, A. C. Ehlinger, W. J. Chazin, J. K. Barton. The [4Fe4S] cluster of human DNA primase functions as a redox switch using DNA charge transport. Science 2017, 355, eaag1789.

57. K. J. McDonnell, J. A. Chemler, P. L. Bartels, E. O'Brien, M. L. Marvin, J. Ortega, R. H. Stern, L. Raskin, G.-M. Li, D. H. Sherman, J. K. Barton, S. B. Gruber. A human MUTYH variant linking colonic polyposis to redox degradation of the [4Fe4S]2+ cluster. Nat. Chem. 2018, 10, 873–880.